Proceedings of DETC' 03
ASME Design Engineering Technical Conferences
and Computers and Information in Engineering Conference
Chicago, Illinois, September 2-6, 2003

DETC2003/DAC-48751

DESIGN OPTIMIZATION OF VEHICLE STRUCTURES FOR CRASHWORTHINESS USING EQUIVALENT MECHANISM APPROXIMATIONS

Karim Hamza
Ph.D. Pre-Candidate, Mechanical Engineering Dept.,
University of Michigan, Ann Arbor, MI 48109-2102
khamza@engin.umich.edu

Kazuhiro Saitou
Assistant Professor, Mechanical Engineering Dept.,
University of Michigan, Ann Arbor, MI 48109-2102
kazu@engin.umich.edu

ABSTRACT

Passenger vehicle crashworthiness is one of the essential vehicle attributes. According to National Highway Traffic Safety Administration (NHTSA), there were over six million vehicle crashes in the United States in the year 2000, which claimed the lives of more than forty thousand persons. Vehicle crashworthiness is difficult to satisfy in a manner appeasing to other design decisions about the vehicle. This paper aims at developing a novel methodology for crashworthiness optimization of vehicle structures. Based on observations of the manner of structural deformation, the authors propose the abstraction of the actual vehicle structure, which is to be represented as a linkage mechanism having special nonlinear springs at the joints. The special springs are chosen to allow the motion of the mechanism to capture the overall motion of the actual vehicle structure. It thus becomes possible to optimize the mechanism, which is an easier task than directly optimizing the vehicle structure. A realization of the optimized mechanism is then performed to obtain an equivalent structure, and then direct optimization of the realized structure is performed for further tuning. The study presented shows the success of the proposed approach in finding better designs than direct optimization while using comparatively less computational resources.

INTRODUCTION

Passenger vehicle crashworthiness is one of the essential attributes that vehicle designers strive to improve in order to satisfy government imposed regulations as well as making the vehicles attractive to potential customers in nowadays' highly competitive markets. Unfortunately, crashworthiness is one of the most difficult attributes to satisfy within reasonable ranges of design parameters. Vehicle traction performance and overall cost generally favor making the structure as lightweight as possible while protection against excessive deformation during crash generally favors a stronger structure. Yet again, other crashworthiness requirements do not favor overly stiff structures, which increase occupant injury risk during sever impacts. As such, a good design for crashworthiness requires the structure to be *stiff enough* to prevent intrusions into sensitive areas such as the passenger cabin and fuel system, but *soft enough* to cushion the impact, all while being lightweight and cost efficient. As the target performance of the structure allows formulating the structural design problem of the vehicle as an optimization problem, such a formulation typically requires lots of iterations in order to find an optimum design. However, vehicle crashworthiness simulation contains noise and is so demanding on computational resources, that many of the traditional optimization techniques are unsuited for such optimization task. Only specialized techniques that emphasize obtaining a good design with only a few iterations are practical. Such specialized techniques generally try to exploit any available information about the design problem in order to decrease the need for performing much iteration.

A review of the literature about crashworthiness optimization is conducted. It may be good to distinguish three main categories of crashworthiness optimization research: i) topology optimization, ii) parametric optimization and iii) development of approximate models for the optimization task. Topology optimization may use material homogenization [1, 2]. Material homogenization optimizes material removal from non-critical zones by optimizing size of microstructure voids. An alternative approach to homogenization is material properties interpolation by using a virtual density parameter, which allows a smooth transition between strong material zones (reinforced regions) and softer material zones, which are foam-filled or voided [3-7]. Some other approaches for optimizing the topology make use of lumped parameter models and/or reduced order lattice models [8]. In general, topology optimization is only useful during the early stages of design, that is, during the conceptual design phase, when many of the dimensions and parameters are not yet accurately known or finalized. The output of topology optimization is a *structural concept* or

shape, which is yet to be groomed into a real design, and must later be re-optimized to get the final dimensions.

Parametric optimization for crashworthiness is generally used for obtaining the final dimensions, which are to be implemented in building the vehicle. In parametric optimization, which requires a prior definition of general shape, a set of variables that are allowed to change within limits are defined by the designer. Then, an optimization technique or algorithm is used to estimate the best values for the variables that best satisfy pre-set performance targets. Parametric optimization may also combine crashworthiness targets along with other disciplines [9]. Parametric Optimization may be classified according to the type of model that is the object of optimization into full vehicle optimization and subsystems optimization. Examples of full vehicle optimization are presented in [9, 10] while examples of subsystems optimization are in [11-13]. The main difficulties in crashworthiness parametric optimization are the noisiness of the numerical simulation and the requirement of massive computational resources to run the detailed nonlinear finite element models (FEM) of the full vehicles or subsystems. As such, the dominant approach in parametric optimization is to use some sort of surrogate model within the main optimization loop. The surrogate model serves to smoothen the noise of the finite element simulation as well as economize the number of times needed to run the finite element analysis. Such approach seems to have good success when the size of the finite element model is small enough to allow for a good number of finite element model evaluations, and the reviewed cases of subsystem optimization are good examples of parameter tuning within a region of interest (local optimization) or global optimization using genetic algorithm [13]. Such success in performing the optimization task is severely limited when full vehicles are considered. The case considered by Mase *et al.* [10] is a for a low speed test (5 mph), in which most of the vehicle parts which are known not to deform were removed from the finite element model. The other case considered by Yang *et al.* [9] required the use of 512 processors running in parallel for 72 hours to perform only two local optimization iterations. Such massive requirement of computational resources is the real challenge, which limits crashworthiness optimization.

Due to the massive requirement of computational resources required for crashworthiness optimization, a fair amount of research is dedicated to finding approximate models that can be used for approximate optimization at a cheap computational cost. The use of such models helps decrease the number of full finite element simulations required to achieve a good design. The most widely used type of approximate models is of the response surface method (including several variations). Examples in the literature are [14-18]. In general, response surface methods are abstracting, in the sense that they completely replace the actual model (finite element) by the meta-model and retain no knowledge of the original system they approximate other than its outputs due to a given set of inputs. Response surface methods are also general purpose and not necessarily specific to structural optimization so the fact that they are relatively easy to use is what accounts for their wide popularity. Another approach, which is less popular than response surface methods, but is specific to structural optimization, is the use of coarse mesh, lumped parameter or lattice models [8, 19-21]. The main difficulty in using lumped models is the realization into an actual design, which is a difficult optimization problem by itself. Thus lumped models find limited practical use other than topology optimization during the conceptual design stage. Other approaches in developing models that have found some applicability include: identification of good reduced models [22], wavelet signal analysis [23] and investigation of possibilities for crash energy absorption by non-structural elements [24]. Of the approximate modeling techniques, the only family of techniques, which seem to find practical application in parametric design optimization, is the response surface methods (RSM). The main disadvantage of RSM is the excessive abstraction of the actual model and the computational resources need to construct the response surface, which must be done by sampling several full FEM simulations.

This paper aims at developing a methodology that is suitable for use in parametric design, yet does not induce too much abstraction of the model as well as requiring less computational resources. The novel idea presented in this paper is that the abstraction of an actual vehicle is done by representing the structure as a linkage mechanism, which has special nonlinear springs at the joints. The nonlinear springs are chosen to allow the motion of the mechanism to capture the overall motion/deformation of the actual vehicle structure. Thus instead of optimizing the full FEM model, optimization of the equivalent mechanism is conducted, which is an easier task. Realization of the optimized mechanism is then performed to obtain back an equivalent structure, which can be further tuned by direct optimization using any of the already established methods.

This paper starts with a review of some of the relevant literature, followed by presentation of the proposed special nonlinear springs/joints that allow approximating a vehicle structure by an equivalent mechanism. Then the overall proposed optimization strategy is presented, followed by two applied case studies to demonstrate the proposed approach. The paper ends in a discussion of the advantages and limitations of the proposed approach and its future extensions.

MECHANISM MODELS OF STRUCTURAL MEMBERS

An interesting observation about the failure modes of thin walled structural members during the crash event is that there are generally two manners of failure, namely: Crushing and Bending. A typical example of crushing shape is shown in Fig. 1. Crushing occurs when the main load on the member is acting in the axial direction and exceeds the plate buckling stress of some portion of the member structural member. The structural member then starts to deform more rapidly in the axial direction as its resistance to deformation drops due to plastic yielding of the material as well as growth of the geometric imperfections or distortions. A typical example of bending shape is shown in Fig. 2. Bending collapse occurs when the bending moment on the structural member causes the stress on the compression side of the thin walled section to exceed the plate buckling stress. Bending collapse happens more gradually as portions of the member cross-section gradually yield whereas during crushing, nearly the whole cross-section yields.

Several curves of the Crushing Resistance Force for different cross-section dimensions of box-sections are plotted in Fig. 3. The data for the plots is generated using LS-DYNA explicit nonlinear finite element (FEM) code [25]. Material

properties and material model are those for mild steel and are given in Table 1. In these FEM simulations, the crashing speed is 1.0 m/s (close to quasi-static). The simulations are in agreement with reported experimental work [26]. A similar set of curves for the bending behavior is shown in Fig. 4. Simulations of Fig. 4 are also in agreement with reported experimental work [11]. It is noted that the FEM simulations were performed on specimens that are short enough so that only one fold of the sheet metal occurs, thereby giving a simpler behavior to be approximated later on in this paper.

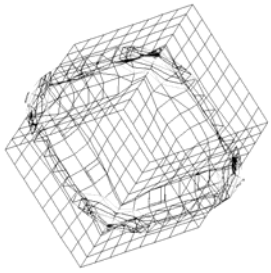

Fig. 1. Typical Crushing Shape of a Box Section

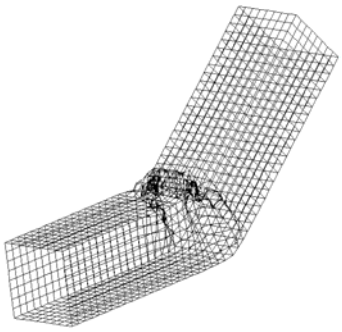

Fig. 2. A Typical Bending Shape of a Box Section

Table 1. Material Properties of Mild Steel used in Models

Young's Modulus	207.0	GPa
Poisson's Ratio	0.3	
Density	7800.0	kg/m^3
Yield Stress	240.0	MPa
Material is assumed to be linear elastic up till yield, then perfectly plastic		

It is observed from Fig. 3 and Fig. 4 that the characteristic curves of the deformation resistance in both crushing and bending have the same general shape. Such shape is characterized by a quick early peak deformation resistance, which is followed by a drop to a lower and nearly steady deformation resistance. In order to achieve successful abstraction of the structural member, an abstracted model must be capable of capturing such behavior.

A nonlinear spring element is proposed. The purpose of the nonlinear spring element is to capture the quasi-static behavior of a thin walled section during crushing (axial spring) or bending (torsional spring). It has been observed that both crushing and bending exhibit similar overall deformation resistance curves, so although the discussion in this section focuses on the crushing resistance force, the same equations are used for the bending resistance moment.

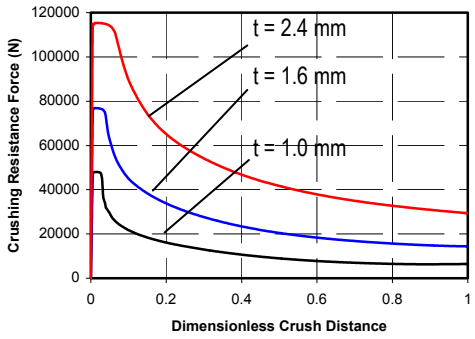

(a) Box Section 50×50 mm

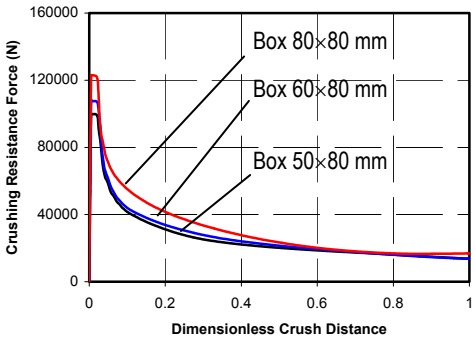

(b) Box Sections, t = 1.6 mm

Fig. 3. Typical Crushing Resistance Force Curves

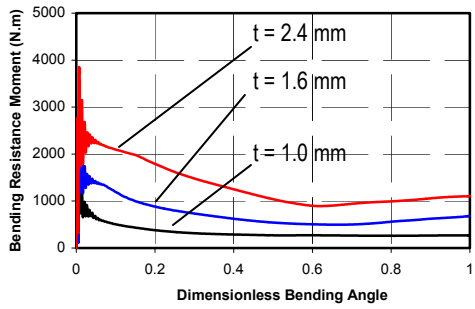

(a) Box Section 50×50 mm

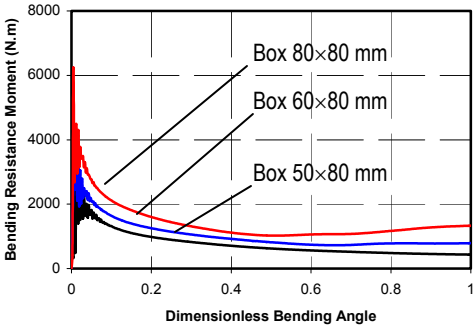

(b) Box Sections, t = 1.6 mm

Fig. 4. Typical Bending Resistance Moment Curves

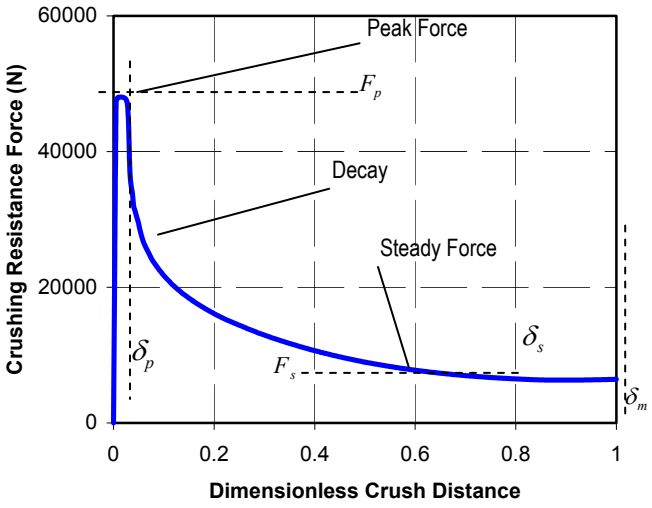

Fig. 5. LS-DYNA Simulation of Crushing Resistance Force Curve of a 50×50m×1.0mm Box Section

Shown in Fig. 5 is the quasi-static crushing resistance force verses axial deformation of a 50mm × 50mm, 1mm thickness, mild steel (properties given in Table 1) box-section. The curve is generated using the nonlinear FEM code LS-DYNA. The following main characteristics are identified:

- Fast rise to the peak force, during which the relation between force and deformation is close to being a simple linear stiffness. Such behavior agrees with what one expects during the early elastic zone.
- Flattened peak occurs in the force verses deformation curve following the fast rise.
- Drop in the crushing resistance force following the peak to become almost steady.

The nonlinear equation of the spring force as a function of the deformation is chosen to generate a closely matching behavior to that observed during FEM simulation of the box section. The following curve characteristics (or "Section Properties") are identified:

- Peak force value (F_p)
- Deformation at which the peak force occurs (δ_p)
- Steady force value at high deformation (F_s)
- Maximum deformation, after which the box section becomes solid (δ_m)

An additional set of parameters is identified in order to further tune the nonlinear spring. The tuning parameters are:

- Fraction of the peak force, during which the section is still in the elastic range (μ_{fe}), thus:

$$F_e = \mu_{fe} F_p \quad \textbf{(1)}$$

  Where F_e is the maximum elastic force

- Fraction of δ_p at which F_e occurs ($\mu_{\delta e}$), thus:

$$\delta_e = \mu_{\delta e} \delta_p \quad \textbf{(2)}$$

  Where δ_e is the deformation at which F_e occurs

- Multiple of δ_p at which the crushing resistance force settles into its steady value ($\mu_{\delta s}$), thus:

$$\delta_s = \mu_{\delta s} \delta_p \quad \textbf{(3)}$$

  Where δ_s is the deformation at which the crushing resistance force settles to within 2% of F_s

A FEM simulation (or an actual physical test) of the quasi-static crushing of a given thin walled section is needed to evaluate F_p, δ_p and F_s. Such necessity is the reason F_p, δ_p and F_s are referred to as "Section Crushing Properties." On the other hand, it is possible to find estimates of μ_{fe}, $\mu_{\delta e}$ and $\mu_{\delta s}$ that are suitable for a wide range of cross-sections. δ_m can be estimated beforehand from the physical length of the spring element.

Due to varying crushing resistance force behavior in the different modes of crushing (elastic, close to peak, steady and solid length) it makes sense to have special functions for each of the crushing modes in their respective zones of the curve (Fig. 6). For a given deformation (δ), the functions for each of the zones are:

- Zone 1: Linear Elastic

$$F_1 = k_e \delta_1 \quad \textbf{(4)}$$

  Where:

$$k_e = \frac{F_e}{\delta_e}$$

$$\delta_1 = \delta$$

- Zone 2: Quadratic Peak

$$F_2 = F_p - k_2 \delta_2^2 \quad \textbf{(5)}$$

  Where:

$$k_2 = \frac{F_p - F_e}{(\delta_p - \delta_e)^2}$$

$$\delta_2 = \delta - \delta_p$$

- Zone 3: Exponential Decay

$$F_3 = F_s + (F_e - F_s)\ e^{-k_3 \delta_3} \quad \textbf{(6)}$$

  Where:

$$k_3 = \frac{4}{(\delta_s - 2\delta_p + \delta_e)}$$

$$\delta_3 = \delta - 2\delta_p + \delta_e$$

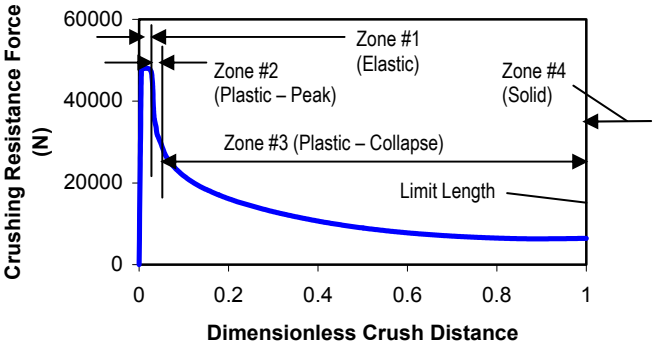

Fig. 6. Zones of the Crushing Resistance Force Curve

- Zone 4: Solid-Length

$$F_4 = F_s + k_s \delta_4 \quad \textbf{(7)}$$

Where:

$$k_s = \mu_s k_e$$

$$\delta_4 = \delta - \delta_m$$

Typical values for δ_m, μ_s, μ_{fe}, $\mu_{\delta e}$ and $\mu_{\delta s}$ are given in Table 2. In order to avoid discontinuity during transition from one zone of the curve to another, the functions to calculate the crushing resistance force in each zone are multiplied by smoothening sigmoid functions [27]. Sigmoid functions are continuously differentiable and present a good alternative to the Step (Hard-Limit) function. A dimensionless plot of the sigmoid function is shown in comparison with the hard-limit function in Fig. 7 and its equation given a preset limit position and magnification constant is given as:

$$sig(\delta \mid \delta_o, \alpha) = \frac{e^{\alpha(\delta - \delta_o)}}{e^{\alpha(\delta - \delta_o)} + e^{-\alpha(\delta - \delta_o)}} \quad \textbf{(8)}$$

Where δ_o is the zero point of the sigmoid function and α is a magnification constant.

The overall equation to compute the crushing resistance force of the nonlinear spring (F_k) is given as:

$$F_k = \sum_{i=1}^{4} \left(sig(\delta \mid \delta_{oi}, \alpha) - sig(\delta \mid \delta_{oi+1}, \alpha) \right) \; F_i(\delta_i) \quad \textbf{(9)}$$

Thus the sigmoid functions provide a smooth fade-in and fade-out for the zone-specific functions and it is possible to prove that the overall curve equation of the nonlinear spring given by equation 9 is continuously differentiable even in its higher derivatives.

Examples of the tuned nonlinear spring equation compared to the original FEM simulation are given in Fig. 8 and Fig. 9. Figure 8 is an example of crushing resistance force and Fig. 9 is an example of bending resistance moment.

It is only on very rare occasions that a spring element in a dynamic system gets loaded in only one direction without partially springing back. Where equation 9 defines the curve equation of the nonlinear spring when deformation is continuously increased in one direction, when the deformation goes into the opposite direction, a different equation should be used, otherwise unrealistic behavior can occur.

Figure 10 shows the proposed unloading scheme. During the dynamic simulation, the code responsible for simulating the nonlinear spring keeps track of the new zero-resistance force point. The zero-resistance force point is computed by projecting a line parallel to the elastic zone curve from the maximum point visited on the curve (Fig. 10). Should unloading occur, it follows that same unloading line. When reloading occurs after the unloading, the force follows the unloading line up till the original force curve (given by Equation 9) then continues along it (Fig. 10).

The nonlinear spring model represented by equation 9 is developed to capture the observed crushing or bending behavior of structural members during quasi-static loading. However a real crash event will almost always be at a speed too high to be judged as quasi-static. Figure 11 shows a comparison of higher speed crushing resistance force to that during quasi-static crushing of the 50mm × 50mm, 1mm thickness, mild steel box-section. Clearly the behavior is not the same.

Table 2. Typical Parameters for Proposed Nonlinear Spring

δ_m	0.85 – 0.95 of the physical length of the structural member
μ_s	2.0 – 5.0
μ_{fe}	0.8 – 0.95
$\mu_{\delta e}$	0.05 – 0.2
$\mu_{\delta s}$	2.5 – 4.0

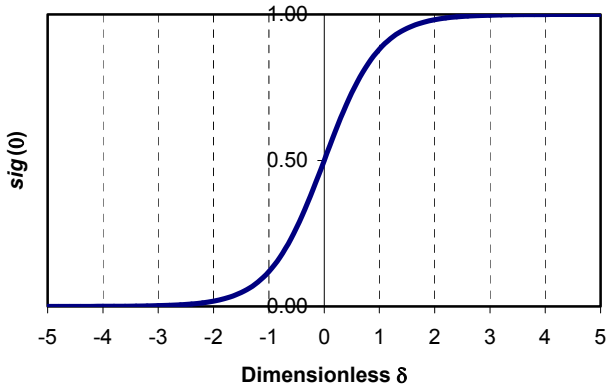

Fig. 7. Dimensionless Plot of the Sigmoid Function

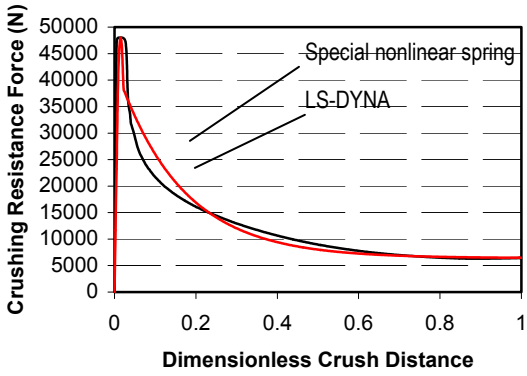

Fig. 8. Crushing Response of the Special Nonlinear Spring

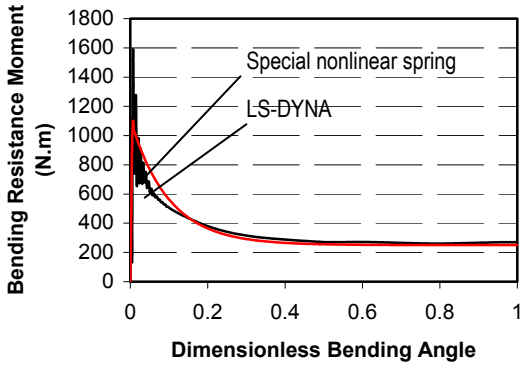

Fig. 9. Bending Response of the Special Nonlinear Spring

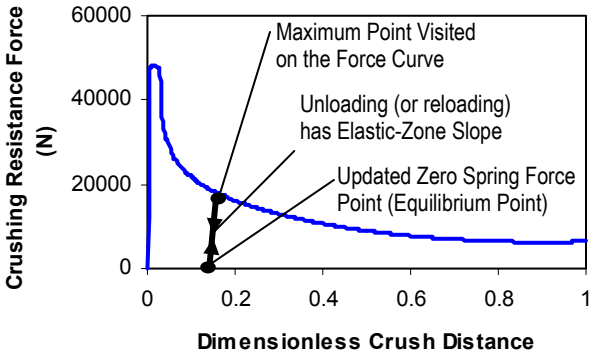

Fig. 10. Unloading of the Special Nonlinear Spring

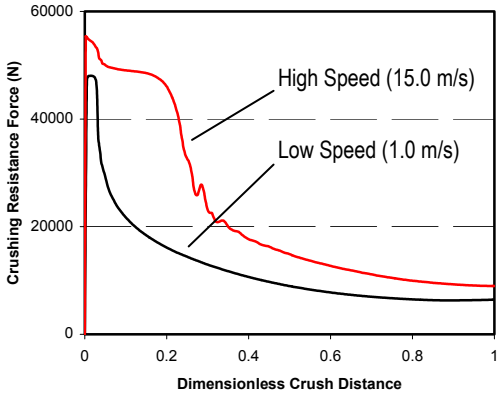

Fig. 11. High Speed Crush of 50×50×1.0mm Box Section

The authors perceive the reason for the different behavior during high and low speed crush to be the effect of inertia of the cross-section, which causes the axial member to act as if it has shorter length, and thus higher stiffness. This is explained by imagining the axial member as a series of masses and springs (Fig. 12). A slow impact force at one side will cause almost equal deformation in all springs along the length of the structural member, while a high speed impact will affect the springs closest to it only before the impact propagates through the structural member (Fig. 12). This explanation of the higher speed crush behavior is supported by observation of the deformed shape of the cross-section during high-speed crush (Fig. 13). The explanation is also supported by the fact that the high speed crushing resistance force tends to remain steady for some time at a value equal to the peak of the low speed crush then dropping to the steady force value of the low speed crush (Fig. 11). Such behavior could very well be the effect of transition between when only a short portion of the structural member is active in the crush, to when the entire structural member is affected by the crush.

To achieve a good model for both high and low crush speed, the authors propose a crush member composed of two masses along a prismatic joint (Fig. 14). The two masses are connected together through a soft nonlinear spring (tuned to the quasi-static behavior of the structural member) and each of the two masses is connected to nodes outside the crush member through stiff nonlinear springs (peak force equal to high speed peak and steady force equal to low speed peak). This proposed crush member would then behave similar to quasi-static behavior during low speed crush, but would also bring about the high-speed characteristics during high-speed crush.

Although it may be possible to develop a similar bending member to capture high and low-speed bending behavior by following a similar approach to the one presented in this section, high-speed bending behavior itself is difficult to characterize. Such difficulty arises because of numerical simulation noisiness, coupling between cross-section bending and cross-section shearing plus high sensitivity to the boundary conditions (manner of structural member fixation and bending load application).

Thus, due to lack of consistent data about high-speed bending behavior, the approximated model presented in this research uses the quasi-static bending characteristics for both high and low speed bending.

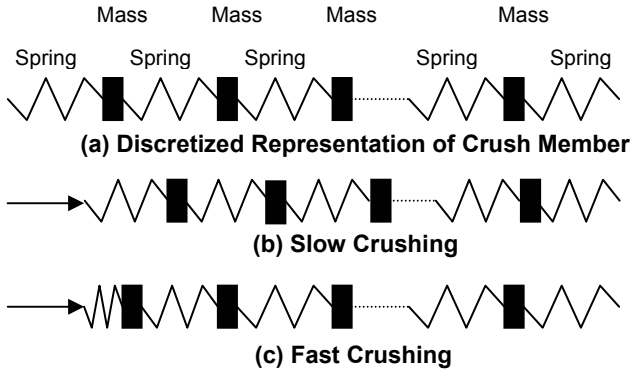

Fig. 12. Discretized Representation of Crush Phenomenon

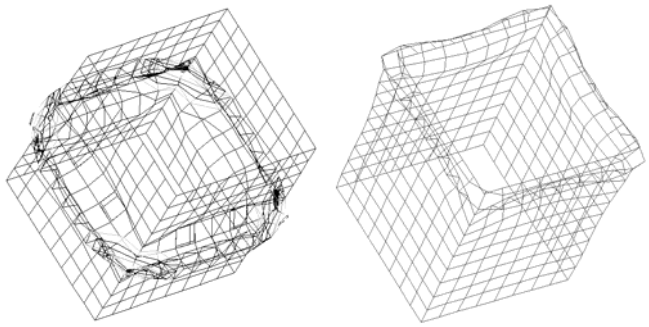

Fig. 13. Effect of Crushing Speed on Deformation Shape

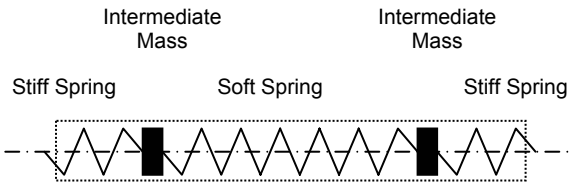

Fig. 14. Proposed Crush Member

PERFORMANCE OF MECHANISM MODELS

The developed nonlinear spring models are to be used in simulating the behavior of an actual set of vehicle structural members during crash, by approximating the structural members as elements of a mechanism, whose joints have these special spring elements. The case study used for testing the proposed model is the main rail of passenger vehicle during the frontal crash event (Fig. 15). Simulation of the crash event is performed using LS-DYNA instead of using an actual crash test. The test is performed three times, each using different cross-section dimensions for the main rail. The tests are referred to as Test #1, Test #2 and Test #3. The main rail data for each of the tests is given in Table 3.

The equivalent mechanism of the main rail is shown in Fig. 16. The identified nonlinear spring constants of the proposed model for the main rail sections are given in Table 4. In general, better overall matching of performance is achieved when using the bending nonlinear springs that are about 10% to 20% weaker that the identified value of the member cross-section. Since the equivalent mechanism can only bend at the revolute joints, using weaker nonlinear bending springs compensates to some extent the tendency of the equivalent mechanism to be unrealistically stiff in bending.

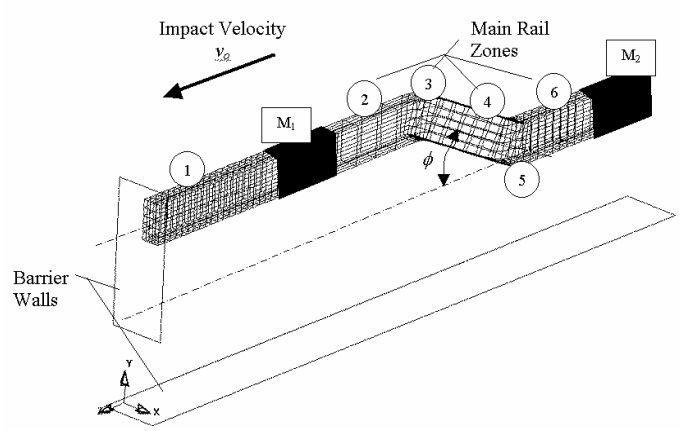

Fig. 15. Finite Element Model of a Vehicle Main Rail

Table 3. Data of Test Main Rails

	Test #1	Test #2	Test #3	Unit
M_1	58.0	58.0	60.0	kg
M_2	130.0	130.0	130.0	kg
v_o	15.0	15.0	15.0	m/s
ϕ	0.451	0.451	0.451	rad
h	50.0	50.0	50.0	mm
b	50.0	50.0	80.0	mm
t_1	1.0	1.0	1.6	mm
t_2	1.0	1.0	1.6	mm
t_3	1.0	2.0	1.6	mm
t_4	1.0	2.0	1.6	mm
t_5	1.0	2.0	1.6	mm
t_6	1.0	2.0	1.6	mm

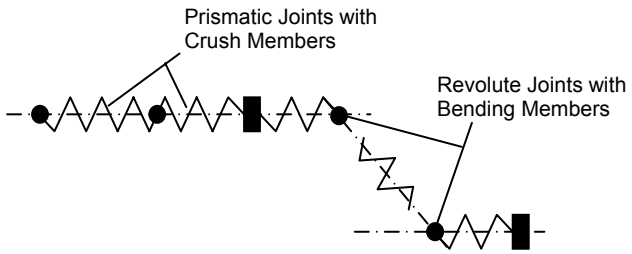

Fig. 16. Equivalent Mechanism Model of the Main Rail

Table 4. Data of Equivalent Mechanisms

	Test #1	Test #2	Test #3	Unit
CM #1 Peak	50000.0	50000.0	105000.0	N
CM #1 Steady	10000.0	10000.0	14000.0	N
CM #2 Peak	50000.0	50000.0	105000.0	N
CM #2 Steady	10000.0	10000.0	14000.0	N
CM #3 Peak	50000.0	50000.0	105000.0	N
CM #3 Steady	10000.0	10000.0	14000.0	N
CM #4 Peak	50000.0	100000.0	105000.0	N
CM #4 Steady	10000.0	15000.0	14000.0	N
CM #5 Peak	50000.0	100000.0	105000.0	N
CM #5 Steady	10000.0	15000.0	14000.0	N
BM #1 Peak	800.0	800.0	1500.0	N.m
BM #1 Steady	500.0	500.0	1100.0	N.m
BM #2 Peak	800.0	800.0	1500.0	N.m
BM #2 Steady	500.0	500.0	1100.0	N.m
BM #3 Peak	800.0	800.0	1500.0	N.m
BM #3 Steady	500.0	500.0	1100.0	N.m
BM #4 Peak	800.0	800.0	1500.0	N.m
BM #4 Steady	500.0	500.0	1100.0	N.m
BM #5 Peak	800.0	1000.0	1500.0	N.m
BM #5 Steady	500.0	650.0	1100.0	N.m
BM #6 Peak	800.0	1000.0	1500.0	N.m
BM #6 Steady	500.0	650.0	1100.0	N.m

Note: CM=Crush Member, BM=Bending Member

Animated display comparisons are shown in Fig. 17 and comparison plots of the engine and passenger cabin motion are given in Fig. 18 and Fig. 19. Fig. 17 presents the *Gross Motion* of the FEM model of the main rail and the comparative motion of the equivalent mechanism. In test case #1, there is an observed downward tilting in the FEM solution using LS-DYNA, which is also observed in the equivalent mechanism. Similarly, behaviors are also observed in test cases #2 and #3. In general, it is observed that simply by taking a *member-by-member* mapping from the full FEM model to the equivalent mechanism model, a remarkably similar overall behavior can be simulated at a relatively low computational cost. Computational cost is lower because solving a mechanism with a few members is computationally less expensive than a FEM model with several thousand elements. These approximate equivalent mechanisms can then used for optimization with reasonable effectiveness. A major advantage of the proposed approach is that it does not introduce too much abstraction as in the case of lumped parameter models and surrogate models.

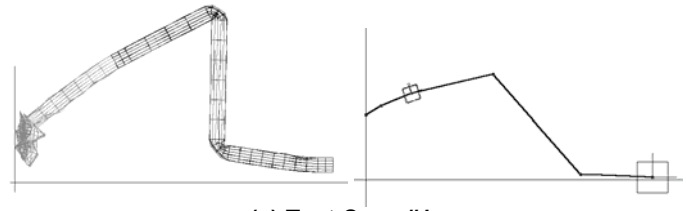

(a) Test Case #1

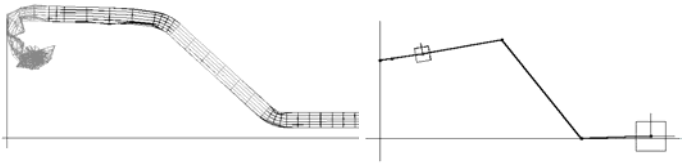

(b) Test Case #2

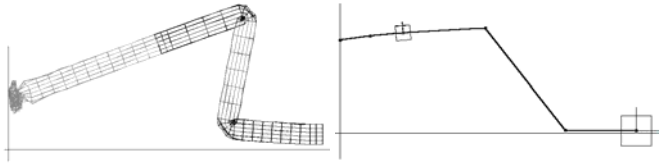

(c) Test Case #3

Fig. 17. Overall deformed shape comparison between FEM simulations using LS-DYNA (left) and the corresponding equivalent mechanisms (right), for test cases 1, 2 and 3

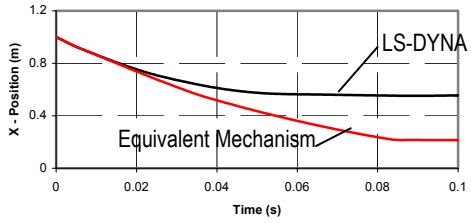

(a) Test Case #1

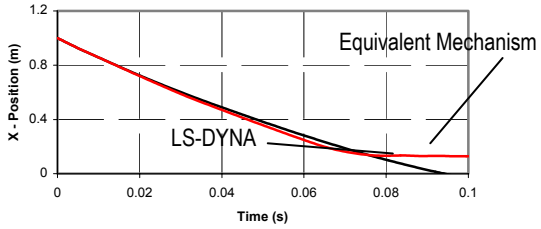

(b) Test Case #2

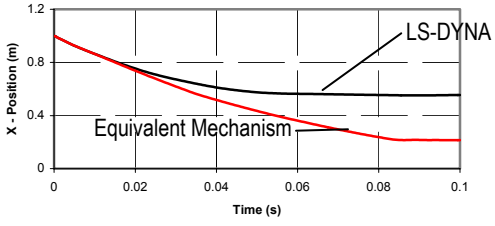

(c) Test Case #3

Fig. 18. X – Location of the Mass M1

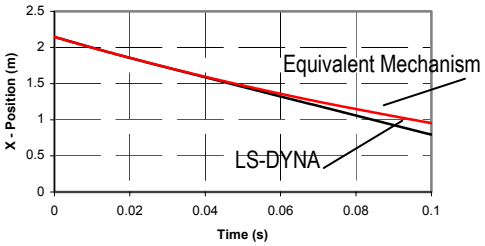

(a) Test Case #1

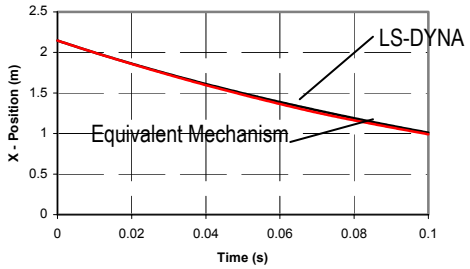

(b) Test Case #2

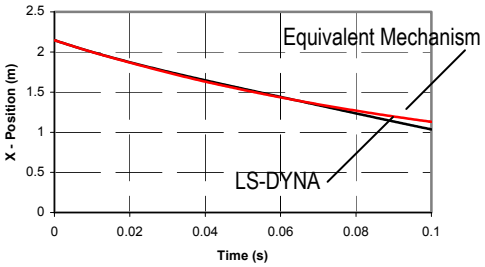

(c) Test Case #3

Fig. 19. X – Location of the Mass M2

OPTIMIZATION SCHEME

Most traditional methods of design optimization for crashworthiness in stages beyond the conceptual design phase are just different variations of *direct optimization* of an accurate FEM model [9]. By *direct optimization*, we mean that the optimization algorithm optimizes a FEM model of the structure or some approximation of it. In some cases, the approximate model may be another FEM model having a coarse mesh. However, the dominant practice in the literature is to use a surrogate model that is constructed by design of experiments (DOE) sampling of the accurate FEM model. The greatest difficulty in traditional approaches is defining the starting point for optimization, or recognizing the region (or regions) where good designs are likely to exist. Such *starting information* is entirely up to the designer's choice according to previous experience.

The approach adopted in this paper employs direct optimization only at the final tuning stage, after a reasonably good design is attained. The scheme for the proposed approach compared to traditional approaches is shown in Fig. 20. The proposed approach follows the following steps

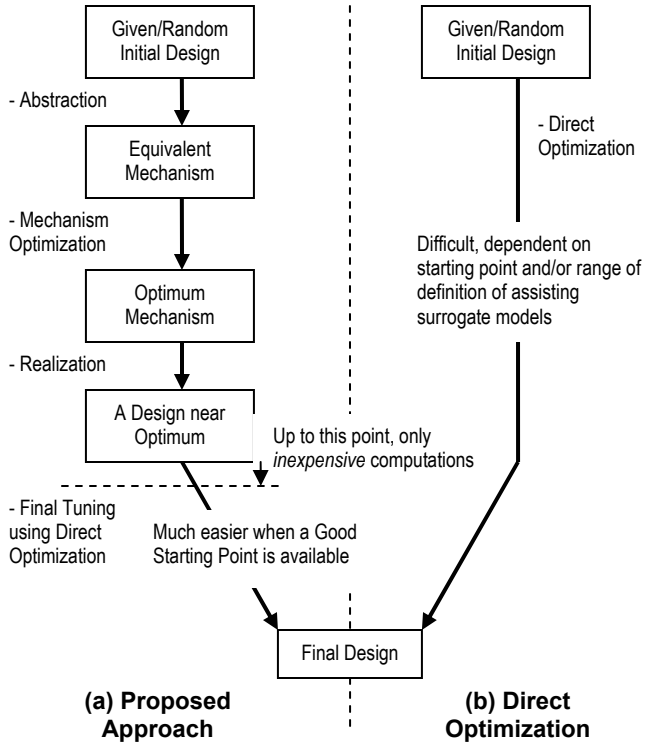

Fig. 20. Proposed Optimization Approach Compared to Direct Optimization

1. Start with an initial design (a guess suggested by the designer).
2. Perform abstraction of the structure by mapping it into an equivalent mechanism.
3. Optimize the equivalent mechanism (which is a much easier task than optimizing the full FEM model).
4. Realize the components of the optimum mechanism and put together into a structure.
5. Perform direct optimization for final design tuning.

Step #2 of the proposed approach is a straightforward operation similar to the Test Examples provided in the previous section. However, there are many possible alternatives for performing steps #3 and #4, based on which, the final outcome may be different. The next section presents a case study that only uses one of the possible options for steps #3 and #4. The case study demonstrates the potential of the proposed design optimization approach in finding better designs, at a comparatively less computational cost. A comparative study of all possible options for steps #3 and #4 is a topic yet to be explored.

CASE STUDY #1

The first case study considered is the optimization of a vehicle main rail (Fig. 15) to minimize the weight, while satisfying some pre-set loading conditions. The main rail is to be optimized using a traditional direct optimization using sequential quadratic programming (SQP) [27] as well as the proposed approach. A schematic diagram of the main rail is given in Fig. 15. There are nine design variables (all assumed continuous), which are listed as:

t_1 through t_6 Shell thickness in zones 1 through 6
h Box-section depth
b Box-section width
ϕ Angle of the main rail

The Objective function is to minimize the total mass of the main rail and is thus given as:

$$f = \rho \frac{(b+h)}{2} \sum_{i=1}^{6} t_i l_i \quad \textbf{(10)}$$

Where: ρ is the material density and l_i is the length of the i^{th} zone.

The rail is crashed against a rigid barrier at an initial velocity of 15.0 m/s. And the crash event is simulated for 100 milliseconds using LS-DYNA software. At the end of the simulation, the rail must satisfy the following design constraints:

$$g_1 = \delta_{12} - 0.95 \le 0 \quad \textbf{(11)}$$

$$g_2 = \delta_{36} - 0.1 \le 0 \quad \textbf{(12)}$$

Where δ_{12} is total deformation along the crash direction in zones 1 and 2 and δ_{36} is total deformation along the crash direction zones 3 through 6

Several trials are performed to find a reasonably good design as a starting point for SQP. The starting and final points of the SQP optimization run are given in Table 5. It is seen that SQP was successful in decreasing the total rail mass. However, many of the design variables did not significantly change, which implies that either the starting point was too good or that SQP terminated because it got stuck at a local optimum.

Following the steps in Fig. 20, an *initial mechanism* is used, which has the same configuration as in Fig. 16. The initial mechanism contains six revolute joints and five prismatic joints, which makes eleven nonlinear springs to optimize. Two design variables are assigned to each spring to represent the peak force (or moment) and steady force (or steady moment) after collapse as a fraction of the peak value. Thus there are a total of twenty-two design variables. The initial values of the design variables are obtained from the abstraction of an overly stiff design and are listed in Table 6.

Table 5. Case Study #1 – Direct Optimization using SQP

	Starting Point	Final Point	Unit
t_1	0.0020	0.00196	m
t_2	0.0012	0.00122	m
t_3	0.0032	0.00312	m
t_4	0.0025	0.00237	m
t_5	0.0032	0.00317	m
t_6	0.0025	0.00237	m
h	0.1400	0.13438	m
b	0.1000	0.09795	m
ϕ	0.5233	0.52896	rad
f	15.4770	14.44680	kg
g_1	-0.2840	-0.28906	m
g_2	-0.0213	-0.00570	m

Since there is no physical practical limit on the design variables of the equivalent mechanism, each variable is allowed to change up to ± 50% of its initial value. The problem

constraints are the same as stated in Equations 11 and 12. However, there is no information about the mass of the mechanism available, so the objective of optimizing the equivalent mechanism is to find the mechanism, which satisfies the constraints, with the *weakest possible* springs at the joints. The intuition behind such formulation is that weak springs should be *realizable* through lighter structures.

Table 6. Case Study #1 – Equivalent Mechanism Optimization using SQP

	Starting Point	Final Point	Unit
CM #1 Peak	540000	112405	N
CM #1 Steady	180000	28355	N
CM #2 Peak	540000	138565	N
CM #2 Steady	180000	41474	N
CM #3 Peak	540000	113770	N
CM #3 Steady	180000	21148	N
CM #4 Peak	540000	111430	N
CM #4 Steady	180000	23841	N
CM #5 Peak	540000	169958	N
CM #5 Steady	180000	31593	N
BM #1 Peak	35000	11114	N.m
BM #1 Steady	8000	1417	N.m
BM #2 Peak	35000	11114	N.m
BM #2 Steady	8000	1417	N.m
BM #3 Peak	35000	11114	N.m
BM #3 Steady	8000	1417	N.m
BM #4 Peak	35000	11114	N.m
BM #4 Steady	8000	1417	N.m
BM #5 Peak	35000	11114	N.m
BM #5 Steady	8000	1417	N.m
BM #6 Peak	35000	11114	N.m
BM #6 Steady	8000	1417	N.m
f	4.80×10^{6}	1.31×10^{6}	kg
g_1	-1.065	-0.388	m
g_2	-0.077	-0.076	m

The initial mechanism is then optimized using SQP. And the final design variables of the final mechanism are given in Table 6. It should be noted that every function and constraints evaluation during the SQP optimization of the mechanism, requires a dynamic simulation. However, the computational cost of simulating a mechanism is lower than full-model nonlinear FEM. As such, the mechanism optimization step could have been performed using some of the more costly global optimization techniques such as genetic algorithm (GA) [28], simulated annealing (SA) [29] and reactive taboo search (RTS) [30].

The realization of the optimum mechanism back into a structure is done this study by multi-objective optimization along two objective functions. The first objective is to minimize an error function of the deviation of the realized structure components relative to the dictated performance (nonlinear springs' peak and steady value) of the optimized mechanism. The second objective is to minimize the realized structure total mass. A Pareto-front for this realization is shown in Fig. 21. The Pareto-front of Fig. 21 is generated using a multi-objective genetic algorithm [31].

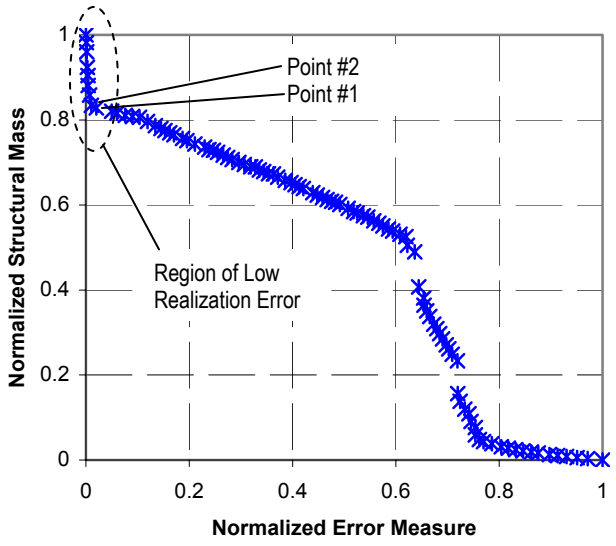

Fig. 21. Case Study #1 – Pareto Front used in realizing the Optimized Mechanism

The region of the Pareto-front where the error function is low provides several potentially good design alternatives. Then, it is possible to pick out some of the Pareto points and test the full FEM model corresponding to them. The FEM simulation results of points #1 and #2 on the Pareto curve of Fig. 21 are listed in Table 7. It is noted that point #2 is a feasible point, that has a better objective function value that the starting point (obtained by rigorous guessing) of the direct SQP optimization.

Up to the realization of the equivalent mechanism, all computations are performed using *computationally inexpensive* models than the full FEM. The final step is to perform direct optimization of the realized mechanism. The realization step is done using SQP on the full FEM model. The start and finish of the SQP run are given in Table 8. The final outcome is a feasible design that is better than the one obtained by direct optimization.

Table 7. Case Study #1 – Realized Designs

	Point #1	Point #2	Unit
t_1	0.0022	0.0022	m
t_2	0.0022	0.002	m
t_3	0.0022	0.0024	m
t_4	0.0022	0.0022	m
t_5	0.0022	0.0024	m
t_6	0.0022	0.0022	m
h	0.1500	0.1500	m
b	0.0700	0.0700	m
ϕ	0.4780	0.4780	rad
f	14.7224	14.8701	kg
g_1	-0.3215	-0.3218	m
g_2	0.0337	-0.0185	m

Table 8. Case Study #1 – Tuning of Point #2 using SQP

	Point #1	Point #2	Unit
t_1	0.0022	0.00212	m
t_2	0.002	0.00207	m
t_3	0.0024	0.00234	m
t_4	0.0022	0.00207	m
t_5	0.0024	0.00231	m
t_6	0.0022	0.00207	m
h	0.1500	0.14536	m
b	0.0700	0.06919	m
ϕ	0.4780	0.48711	rad
f	14.8701	13.70870	kg
g_1	-0.3218	-0.30129	m
g_2	-0.0185	-0.00192	m

CASE STUDY #2

The second case study considered is that of frontal crashworthiness optimization considering both the mid rail (main) and the lower rail of a vehicle (Fig. 22). Similar to the first case study, the objective is to minimize the weight, while satisfying some pre-set loading conditions. The main and lower rails are to be optimized using SQP as well as the proposed approach. A schematic diagram of the main rail is given in Fig. 22. There are eleven design variables, which are listed as:

t_1 through t_7 Shell thickness in zones 1 through 7

h_1 Box-section depth in zones 1, 2, 3, 4

b_1 Box-section width in zones 1, 2, 3, 4

h_2 Box-section depth in zones 5, 6

b_2 Box-section width in zones 5, 6

The Objective function is to minimize the total mass of the main rail and is thus given as:

$$f = \rho \sum_{i=1}^{6} \frac{(b_i + h_i)}{2} t_i l_i \qquad \textbf{(13)}$$

The system is crashed against a rigid barrier at an initial velocity of 15.0 m/s. And the crash event is simulated for 100 milliseconds using LS-DYNA software. At the end of the simulation, the design constraints are:

$$g_1 = \delta_{13} - 0.95 \le 0 \qquad \textbf{(14)}$$

$$g_2 = \delta_4 - 0.1 \le 0 \qquad \textbf{(15)}$$

Where δ_{13} is total deformation along the crash direction in zones 1 through 3 and δ_4 is total deformation along the crash direction zone 4

Several trials are performed to find a reasonably good design as a starting point for SQP. The starting and final point of the SQP optimization run is given in Table 9. The final point obtained by SQP shows success in decreasing the objective function, while maintaining feasibility, however, there is not necessarily the best attainable design.

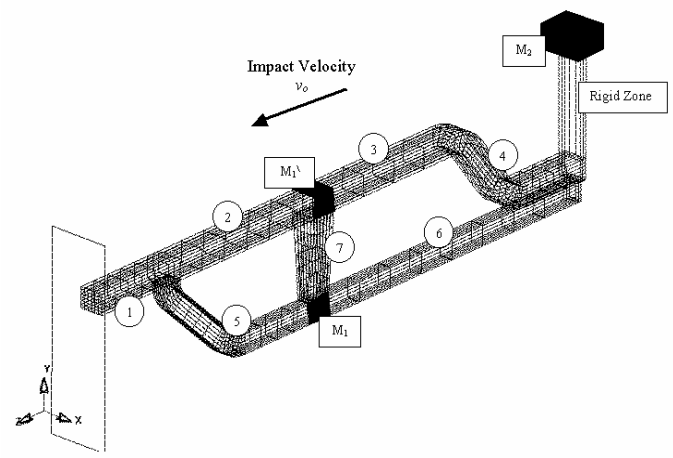

Fig. 22. Finite Element Model of a Vehicle Main and Lower Rails

Table 9. Case Study #2 – Direct Optimization using SQP

	Starting Point	Final Point	Unit
t_1	0.0045	0.00435	m
t_2	0.0022	0.00169	m
t_3	0.0045	0.00453	m
t_4	0.0045	0.00367	m
t_5	0.0045	0.00448	m
t_6	0.0045	0.00450	m
t_7	0.0046	0.00460	m
h_1	0.1200	0.11612	m
b_1	0.8000	0.07128	m
h_2	0.1000	0.09129	m
b_2	0.1000	0.09551	m
f	41.1700	35.59030	kg
g_1	-0.0966	-0.09692	m
g_2	-0.0467	-0.00043	m

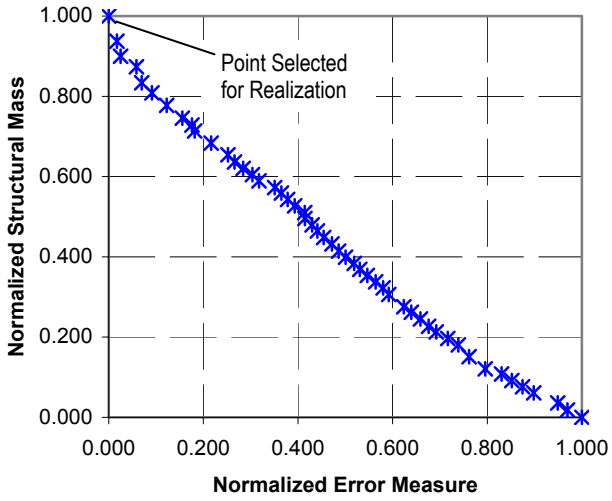

Fig. 23. Case Study #2 – Pareto Front used in realizing the Optimized Mechanism

Table 10. Case Study #2 – Equivalent Mechanism Optimization using SQP

	Starting Point	Final Point	Unit
CM #1 Peak	431620	215810	N
CM #1 Steady	88850	22206	N
CM #2 Peak	173040	86520	N
CM #2 Steady	31400	7849	N
CM #3 Peak	431620	215810	N
CM #3 Steady	88850	22206	N
CM #4 Peak	431620	215810	N
CM #4 Steady	88850	22206	N
CM #5 Peak	435000	217500	N
CM #5 Steady	90750	22687	N
CM #6 Peak	435000	217500	N
CM #6 Steady	90750	22687	N
CM #7 Peak	435000	217500	N
CM #7 Steady	90750	22687	N
BM #1 Peak	16000	8000	N.m
BM #1 Steady	12000	3000	N.m
BM #2 Peak	5600	2800	N.m
BM #2 Steady	2400	600	N.m
BM #3 Peak	16000	8000	N.m
BM #3 Steady	12000	3000	N.m
BM #4 Peak	16000	8000	N.m
BM #4 Steady	12000	3000	N.m
BM #5 Peak	12000	6000	N.m
BM #5 Steady	8000	2000	N.m
BM #6 Peak	12000	6000	N.m
BM #6 Steady	8000	2000	N.m
BM #7 Peak	12000	6000	N.m
BM #7 Steady	8000	2000	N.m
f	1.61×10^{7}	1.42×10^{7}	kg
g_1	-0.158	-0.041	m
g_2	-0.041	-0.057	m

Table 11. Case Study #2 – Fine Tuning of Realized Mechanism using SQP

	Starting Point	Final Point	Unit
t_1	0.0024	0.00454	m
t_2	0.0018	0.00060	m
t_3	0.0026	0.00063	m
t_4	0.0030	0.00453	m
t_5	0.0038	0.00452	m
t_6	0.0039	0.00446	m
t_7	0.0028	0.00460	m
h_1	0.1440	0.06040	m
b_1	0.0830	0.09906	m
h_2	0.0730	0.11974	m
b_2	0.0650	0.04134	m
f	26.2926	27.84080	kg
g_1	-0.0967	-0.05393	m
g_2	0.0853	0.00052	m

Following the steps described in Case Study #1, an equivalent mechanism of the starting point, containing seven prismatic and seven revolute joint values, is optimized using SQP. The mechanism optimization results are given in Table 10. The mechanism realization is performed by selecting a point in the neighborhood of the highlighted point in Fig. 23. It is observed that as more load paths exist in the structure, the realization of a mechanism into a corresponding structure becomes more difficult and dependent the way the error function in Fig. 23 is defined. The mechanism realization in the second case study is performed by selecting a point from the Pareto curve, that has a low value of the error function, then exploring its neighborhood for better designs. Tuning of the point obtained from the realized mechanism is performed using SQP and presented in Table 11. It is observed that the tuning optimization run adjusts the realized mechanism, slightly sacrificing on the objective function, to gain feasibility. The final design is significantly better than the one obtained by direct optimization using SQP alone.

DISCUSSION

The approach proposed in this research falls under the category of using approximate meta-models of the more accurate full FEM model to achieve crashworthiness optimization. Unlike the response surface methods and their different variations, which are general purpose for any sort of problem, the proposed approach is specifically tailored for structural crashworthiness, and is based on exploiting prior knowledge of the crash phenomenon.

One possible way to understand the proposed approach is to think of it as a *superset* of the lumped parameter models. Since it is up to designer (so far), to determine the shape and connectivity of the equivalent mechanism to the structure in question, one possible equivalent mechanism (a subset of all possible equivalent mechanisms) is to choose only the main masses (such as engine, cabin, driveline, …etc.) and connect them by nonlinear springs. Such a choice will simply be the lumped parameter model. On the other hand, the real power of the proposed approach, which allows its use for parametric design optimization, is the existence of a one to many or one to one mapping between the actual structure and possible equivalent mechanisms. That is, it seems possible to approximate the gross behavior of any vehicle structure by one or more equivalent mechanisms. Moreover, it is relatively easy to obtain a good guess of the appropriate equivalent mechanism, simply by *translating* the individual components of the structure.

After abstracting the vehicle structure to its equivalent mechanism, optimization of the mechanism is performed to satisfy and/or improve the set of desired performance criteria. The optimization of the mechanism is an easier task than optimizing the full FEM model of the vehicle structure because of the computational resources required for simulating a *candidate mechanism* are appreciably less than a candidate FEM model. When an optimum mechanism is obtained, it must be realized into its equivalent structure. Although several realization approaches are possible, the one presented in this study uses only low computational cost models to obtain approximate realizations. It is seen that some of the obtained realizations are already fairly good designs, which can be further tuned using conventional methods to obtain a better final design.

An important observation is that the realization of the optimized mechanism is of prime importance to the effectiveness of the proposed approach. One of the essential factors that contribute to successful realization of the optimized mechanism is the definition of the error measure between the optimized mechanism and its realization. Having a unidirectional error, in which, if the realized member is

stronger than the equivalent mechanism incurs no penalty works well in simpler constructions, which don't have many load paths (such as case study #1). However, when multiple load paths exist, an extra strong member at some location can actually disrupt the crash event sequence and thus worsen the overall crashworthiness. On the other hand, if a bi-directional error function is used for all members, there will be a tendency of the realization to produce structures that are too weak (since they have same error measure but lower objective function than a correspondingly strong structure).

Tables 12 and 13 summarize the outcome of the conventional and proposed optimization approaches for both case studies. It can be seen, that the proposed approach allows for finding fairly good designs using only few full FEM model simulations, or better designs than conventional methods (Direct optimization using SQP) while utilizing a comparative number of full FEM model simulations. Thus, the effectiveness of the proposed approach is established for the considered case studies.

Table 12. Summary of Case Study #1 Results

	Conventional – Starting Point	Proposed – Realized Mechanism	Conventional – Final Point	Proposed – Final Point
Number of Full FEM Runs	≈ 10	≈ 10	≈ 220	≈ 210
f	15.4770	14.8701	14.44680	13.70870
g_1	-0.2840	-0.3218	-0.28906	-0.30129
g_2	-0.0213	-0.0185	-0.00570	-0.00192

Table 13. Summary of Case Study #2 Results

	Conventional – Starting Point	Prop. – Real. Mechanism	Conventional – Final Point	Proposed – Final Point	Found by Inspection
Number of FEM Runs	≈ 10	≈ 30	≈ 130	≈ 130	–
f	41.1700	26.2926	35.5903	27.8408	25.5022
g_1	-0.0966	-0.0967	-0.0969	-0.0539	-0.0552
g_2	-0.0467	0.0853	-0.0004	0.0005	-0.0029

It is noted that the results of the current tests are not quite the end of the story. For instance the authors found another design (last column in Table 13), by simple inspection of the design space to match a preferred crash sequence (that the frontal portion should be crushed first). The design obtained by inspection has the same values of the design variables as the final point using the proposed method (Table 11), but the sheet thickness t_1 is reduced to 1.0 mm. The design obtained by inspection is seen to be strictly better than the final obtained result using the proposed method. This observation highlights the importance of observing the crash event itself as a means to guiding the optimization and not relying solely on standard automated algorithms. Further work would include incorporation of *preferred crash sequences* to guide the optimization search in the newly emerging methodology presented in this paper.

CONCLUSION

A new approach to crashworthiness optimization of passenger vehicle structures is presented. The proposed approach goes through several steps that help find a good design, while utilizing only an abstracted equivalent mechanism model of the vehicle structure. The realized mechanism by itself is a fairly good design, and can be further improved by local optimization. Thus, the proposed approach helps a designer obtain a good design using comparatively little computational resources than other methods. The presented studies show the feasibility and advantage of the approach.

So far, the proposed approach is tested only on vehicle substructures that can be represented by a two-dimensional mechanism. Extending the implementation to three-dimensional mechanisms is essential prior to testing it on full vehicle structures. Application of the proposed approach to full vehicles would be of much more attractiveness to vehicle designers and is the ultimate goal of this research. Three-dimensional implementation of the proposed approach and using it for global and/or multi-objective optimization of full vehicles is to be pursued in future work.

Another advantage to the proposed methodology is that the equivalent mechanisms can be viewed as *physical surrogate* models. This allows for incorporating criteria such as matching of preferred crash sequences into the optimization algorithm to enhance the search efficiency and quality. Such enhancement will also be pursued in future work.

ACKNOWLEDGMENTS

This research is sponsored by Nissan Technical Center North America, Inc.

REFERENCES

[1] Mayer, R. R., Kikuchi, N. and Scott, R. A., 1996, "Application of Topological Optimization Techniques to Structural Crashworthiness," International Journal for Numerical Methods in Engineering, Vol. 39, pp. 1383-1403.

[2] Mayer, R. R., 2001, "Application of Topological Optimization Techniques to Automotive Structural Design," Proceedings of the ASME 2001 International Mechanical Engineering Congress and Exposition, November 11-16, New York, NY, IMECE 2001 / AMD 25458.

[3] Luo, J., Gea, H. C. and Yang, R. J., 2000, "Topology Optimization for Crush Design," Proceedings of the 8th AIAA/USAF/NASA/ISSMO Symposium on Multidisciplinary Analysis and Optimization, September 6-8, Long Beach, CA, AIAA Paper Number: AIAA-2000-4770.

[4] Mayer, R. R., Maurer, D. and Bottcher, C., 2000, "Application of Topological Optimization Program to the Danner Test Simulation," Proceedings of the ASME 2000 Design Engineering and Technical Conference, September 10-13, Baltimore, Maryland, DETC 2000 / DAC 14292.

[5] Gea, H. C. and Luo, J., 2001, "Design for Energy Absorption: A Topology Optimization Approach," Proceedings of the ASME 2001 Design Engineering and Technical Conference, September 9-12, Pittsburgh, PA, DETC 2001 / DAC 21060.

[6] Soto, C. A., 2001, "Optimal Structural Topology Design for Energy Absorption: A Heurtistic Approach," Proceedings of the ASME 2001 Design Engineering and Technical Conference, September 9-12, Pittsburgh, PA, DETC 2001 / DAC 21126.

[7] Soto, C. A., 2001, "Structural Topology for Crashworthiness Design by Matching Plastic Strain and Stress Levels," Proceedings of the ASME 2001 International Mechanical Engineering Congress and Exposition, November 11-16, New York, NY, IMECE 2001 / AMD 25455.

[8] Soto, C. A. and Diaz, A. R., 1999, "Basic Models for Topology Design Optimization in Crashworthiness Problems," Proceedings of the ASME 1999 Design Engineering and Technical Conference, September 12-15, Las Vegas, Nevada, DETC 99 / DAC 8591.

[9] Yang, R. J., Gu, L., Tho, C. H. and Sobieski, J., 2001, "Multidisciplinary Optimization of a Full Vehicle with High Performance Computing," Proceedings of the American Institute of Aeronautics and Astronautics 2001 Conference, pp. 688-698, AIAA Paper Number: AIAA-2001-1273.

[10] Mase, T., Wang, J. T., Mayer, R., Bonello, K. and Pachon, L., 1999, "A Virtual Bumper Test Laboratory for FMVR 581," Proceedings of the ASME 1999 Design Engineering and Technical Conference, September 12-15, Las Vegas, Nevada, DETC 99 / DAC 8572.

[11] Han, J. and Yamada, K., 2000, "Maximization of the Crushing Energy Absorption of the S-Shaped Thin-Walled Square Tube," Proceedings of the 8th AIAA/USAF/NASA/ISSMO Symposium on Multidisciplinary Analysis and Optimization, September 6-8, Long Beach, CA, AIAA Paper Number: AIAA-2000-4750.

[12] Kurtaran, H., Omar, T. and Eskandarian, A., 2001, "Crashworthiness Design Optimization of Energy-Absorbing Rails for the Automotive Industry," Proceedings of the ASME 2001 International Mechanical Engineering Congress and Exposition, November 11-16, New York, NY, IMECE 2001 / AMD 25452.

[13] Chen, S., 2001, "An Approach for Impact Structure Optimization using the Robust Genetic Algorithm," Finite Elements in Analysis and Design, Vol. 37, pp. 431-446.

[14] Yang, R. J., Tho, C. H., Wu, C. C., Johnson, D. and Cheng, J., 1999, "A Numerical Study of Crash Optimization," Proceedings of the ASME 1999 Design Engineering and Technical Conference, September 12-15, Las Vegas, Nevada, DETC 99 / DAC 8590.

[15] Shi, Q. Hagiwara, I. and Takashima, F., 1999, "The Most Probable Optimal Design Method for Global Optimization," Proceedings of the ASME 1999 Design Engineering and Technical Conference, September 12-15, Las Vegas, Nevada, DETC 99 / DAC 8635.

[16] Yang, R. J., Gu, L., Liaw, L., Gearhart, C., Tho, C. H., Liu, X. and Wang, B. P., 2000, "Approximations for Safety Optimization of Large Systems," Proceedings of the ASME 2000 Design Engineering and Technical Conference, September 10-13, Baltimore, Maryland, DETC 2000 / DAC 14245.

[17] Yang, R. J., Wang, N., Tho, C. H., Bobineau, J. P. and Wang, B. P., 2001, "Metamodeling Development for Vehicle Frontal Impact Simulation," Proceedings of the ASME 2001 Design Engineering and Technical Conference, September 9-12, Pittsburgh, PA, DETC 2001 / DAC 21012.

[18] Redhe, M. and Nilsson, L., 2002, "Using Space Mapping and Surrogate Models to Optimize Vehicle Crashworthiness Design," Proceedings of the 9th AIAA/ISSMO Symposium on Multidisciplinary Analysis and Optimization, September 4-6, Atlanta, Georgia, AIAA Paper Number: AIAA-2002-5536.

[19] Bennett, J. A., Lust, R. V. and Wang, J.T., 1991, "Optimal Design Strategies in Crashworthiness and Occupant Protection," ASME AMD-Vol. 126, pp. 51-66.

[20] Chellappa, S. and Diaz, A., "A Multi-Resolution Reduction Scheme for Structural Design," Proceeding of the NSF 2002 Conference, January 2002, pp. 98-107.

[21] Ignatovich, C. L. and Diaz, A., 2002, "Physical Surrogates in Design Optimization for Enhanced Crashworthiness," Proceedings of the 9th AIAA/ISSMO Symposium on Multidisciplinary Analysis and Optimization, September 4-6, Atlanta, Georgia, AIAA Paper Number: AIAA-2002-5537.

[22] Jaskulski, J. and Mekhilef, M., 1999, "Side Impact Crash Modeling: Development of a Numerical Identification Tool using Optimization Methods," Proceedings of the ASME 1999 Design Engineering and Technical Conference, September 12-15, Las Vegas, Nevada, DETC 99 / DAC 8698.

[23] Gearhart, C., 1999, "Application of Wavelet Based Signature Analysis in Designing for Crashworthiness," Proceedings of the ASME 1999 Design Engineering and Technical Conference, September 12-15, Las Vegas, Nevada, DETC 99 / DAC 8592.

[24] Saha, N. K. and Bhojan, R., 2001, "Influence of Chassis and Driveline Components in Vehicle Frontal Crash," Proceedings of the ASME 2001 International Mechanical Engineering Congress and Exposition, November 11-16, New York, NY, IMECE 2001 / AMD 25434.

[25] LSTC, 2001, LS-DYNA Software Manuals, Livermore Software Technology Corporation, Livermore, CA, USA.

[26] Koanti, R. P. and Caliskan, A. G., 2001, "Stochastic Applications in Crashworthiness," Proceedings of the ASME 2001 International Mechanical Engineering Congress and Exposition, November 11-16, New York, NY, IMECE 2001 / AMD 25433.

[27] MathWorks, 2001, MatLab 6 Documentation, MathWorks Inc., Natick, MA, USA.

[28] Goldberg, D., 1989, "Genetic Algorithms in Search, Optimization and Machine Learning," Addison-Wesley Inc.

[29] Michalewiz, Z. and Fogel, D. B., 2000, "How to Solve it: Modern Heuristics," Springer-Verlag Berlin Heidelberg, New York.

[30] Battiti, R. and Tecchiolli, G., 1994, "The Reactive Tabu Search," ORSA Journal on Computing, Vol. 6, pp. 126-140.

[31] Coello, C. A., Veldhuizen, D. A. and Lamont, G. B., 2002, "Evolutionary Algorithms for Solving Multi-Objective Problems," Kluwer Academic / Plenum Publishers, New York.

